34th Annual International Conference of the IEEE EMBS
San Diego, California USA, 28 August - 1 September, 2012

A new image reconstruction algorithm for real-time monitoring of conductivity and permeability changes in Magnetic Induction Tomography

Jorge Caeiros[1], Raul C. Martins[2] and Bruno Gil[1]

***Abstract*— A linear image reconstruction algorithm for solving the Magnetic Induction Tomography inverse problem is presented. It's an optimization process to determine a reconstruction matrix that does the best mapping between a set of training parameter vectors and their respective measurements dictated by a forward model. It allows the simultaneous 3D reconstructions of the electric conductivity, electric permittivity and magnetic permeability. The results were compared with the ones obtained from a single-step regularized Gauss-Newton method and a reduction of 15% in the image error was verified. The behavior of the developed algorithm in a simulated clinical environment was also assessed using a realistic bioimpedance model of the human head, derived from a high resolution magnetic resonance image.**

***Index Terms*— Magnetic Induction Tomography, Linear Reconstruction, Passive Electrical Properties.**

I. Context

Magnetic Induction Tomography (MIT) is a non-invasive imaging modality based on the eddy current effect. Its applications range from nondestructive testing [1], to a more recent trend, the medical field (e.g. [2–5]). It aims to use the differences of the passive electric properties (PEP) of tissues to form tomographic images of the human body, while exploiting the inherent advantages of this technology, such as its low cost, contactless nature, high temporal resolution and the fact that the magnetic field can penetrate deeply within biological tissues.

The electrical conductivity (σ), dielectric permittivity (ϵ) and magnetic permeability (μ) are the PEP with greater diagnostic relevance in the medical field. Most studies are only focused on reconstructing the electrical properties of the medium (e.g. [2–5]). The assessment of the magnetic permeability is most often negleted but it could play a very important role in the diagnosis of pathologies that affect the tissue's magnetic properties, an example of which is hemochromatosis where the development of iron overloads occurs in the liver [6].

The image reconstruction in MIT is an ill-posed and non-linear inverse problem. The 3D PEP map is inferred by a set of electromotive force (emf) measurements acquired by sensing coils placed around the periphery of the medium, when a time harmonic current is fed to a source coil. This produces a primary magnetic field that induces eddy currents within the object, which in turn, due to the low conductivity of biological tissues, generates a secondary magnetic field of a much smaller amplitude. The measurements are dictated by the PEP distribution and can be predicted by a a forward model based on a set of electromagnetic partial differential equations.

The inverse problem is conventionally solved iteratively (e.g. in [2, 9, 10]). The material coefficient map in each iteration is refined by resorting to the forward model that determines the solution of several eddy current problems and simulates the set of measurements to be compared to the real ones. Although iterative methods based on the sensitivity analysis using the reciprocity theorem and resulting adjoint fields [7] are available, the overall time of each iteration is still large. The problem can however be tackled by using linear reconstruction algorithms, which assume that small perturbations of the material parameter map translate to linear changes in the acquired measurements. They produce images on a much shorter ammount of time, allowing the technology to be used for monitoring several physiological parameters such as cardiopulmonary functions, brain ischeamia or hemorrage. Their main disadvantage is a degraded spatial resolution when compared to non-linear methods. However, they may be better suited for reconstructions based on experimental data because the measurement noise and geometric uncertainty could prevent stable results with iterative algorithms.

II. Theoretical Background

A. Forward Problem

The MIT forward problem was addressed by a framework based on the conformal Finite Integration Technique (cFIT), using an adaptive and multi-level orthogonal dual-grid complex $(G, \tilde{G})$. The governing equations are the Ampère's law and continuity equation, written in terms of the magnetic vector potential and electrical scalar potential. The electrical conductivity and magnetic permeabilitty are combined in a single complex entity $\zeta = \sigma + i\omega\epsilon$. Using FIT terminology [8], the equations are respectively

$$\widetilde{\mathbf{C}}\mathbf{M}_{\mu}^{-1}\mathbf{C}\,\widehat{\mathbf{a}} + i\omega\mathbf{M}_{\zeta}(\mathbf{G}\boldsymbol{\phi} + \widehat{\mathbf{a}}) = \widehat{\widehat{\mathbf{j}}}_s, \tag{1}$$

$$\widetilde{\mathbf{S}}[i\omega(\mathbf{G}\phi + \widehat{\mathbf{a}})] = 0, \tag{2}$$

where $\mathbf{C}$ and $\mathbf{G}$ are respectively the discrete curl and gradient operators defined in the main grid G, $\widetilde{\mathbf{C}}$ and $\widetilde{\mathbf{S}}$ the curl

[1]J. Caeiros and B. Gil are with the Telecommunications Institute, Lisbon, Portugal jorge.caeiros@lx.it.pt

[2]R. C. Martins is with the Department of Bioengineering, Instituto Superior Técnico, Telecommunications Institute,Lisbon, Portugal rcmartins@ist.utl.pt

and divergence operators defined in the dual grid $\tilde{G}$, $\widehat{\mathbf{a}}$ and ϕ denote respectively the integral of the magnetic vector potential and electric scalar potential along the edges or over the cell volumes of G, and $\widehat{\widehat{\mathbf{j}}}_s$ reflects the integral of the source current density, with angular frequency ω, along the facets of $\tilde{G}$. $\mathbf{M}_\mu$ and $\mathbf{M}_\zeta$ are diagonal matrices representing respectively the magnetic permeability and complex electrical conductivity distribution on the double grid complex. The induced emf is computed by integrating the projection of the magnetic vector potential over the sensing coil's path.

B. Inverse Problem

The proposed linear image reconstruction algorithm is based on [11] and the objective is to determine a reconstruction matrix using a finite difference approximation to the Fréchet derivative. The sensitivity of the measurements is computed by inducing perturbations in the PEP maps being estimated. These perturbations are carried out using a spherical target, placed in several positions spread uniformly across the space being estimated in order to avoid biased reconstructions. The number of these positions should be higher than the number of independent measurement data points available. The reconstruction matrix is determined as the one that minimizes the following quadratic norm function,

$$f(\mathbf{R}) = ||\mathbf{X_t} - \mathbf{R}\mathbf{Y_t}||^2, \tag{3}$$

where $\mathbf{R}$ is the linear reconstruction matrix, $\mathbf{X_t}$ corresponds to the horizontal concatenation of the perturbed maps and $\mathbf{Y_t}$ the corresponding measurements predicted by the forward model. The size of $\mathbf{X_t}$ is $N \times N'$ and $\mathbf{Y_t}$ is $L \times N'$, where N is the number of parameters to be inferred, L the number of measurements and N' the number of target positions. Experimental measurement errors were simulated by adding 5% Gaussian noise to all data. The solution for $\mathbf{R}$ of equation (3) has the following expression,

$$\mathbf{R} = \mathbf{X_t}\mathbf{Y_t}^T(\mathbf{Y_t}\mathbf{Y_t}^T)^{-1}. \tag{4}$$

Increasing the number of target positions doesn't actually translate to a substantial increase in the resolution time of (4), since the only time consuming step consists in the computation of the inverse of a matrix whose size is only dependent on the number of measurements. This makes the implementation of this method in parallel computing highly tempting as each position of the perturbation target can be handled independently, therefore taking advantage of multicore CPU or GPU computing. The time limitation step thus resides in the forward problem solver, which has already been fairly optimized.

The single step Gauss-Newton (GN) method was also implemented for cross-checking the results. It is an optimization algorithm that minimizes the following error functional [2, 9]

$$\epsilon(\mathbf{p}) = ||\mathbf{V_m} - \mathbf{F}(\mathbf{p})||^2 + \alpha||\mathbf{L}(\mathbf{p})||^2, \tag{5}$$

where $\mathbf{F}$ is a forward operator that maps the material properties vector, $\mathbf{p}$, onto virtual measurements, $\mathbf{V_m}$ is the measurement data and $\mathbf{L}$ is the regularization matrix, which in this paper consists in a discrete approximation of the laplacian operator. α is the regularization parameter and $\mathbf{p}$ corresponds to the vertical concatenation of the complex conductivity and magnetic permeability vectors, such that $\mathbf{p} = [\boldsymbol{\zeta}; \boldsymbol{\mu}]$. The solution $\mathbf{p}$ that minimizes (5) has a closed form given by [2, 9, 10]

$$\delta\mathbf{p} = (\mathbf{S}^T\mathbf{S}+\alpha^2\mathbf{L}^T\mathbf{L})^{-1}(\mathbf{S}^T(\mathbf{V_m}-\mathbf{F}(\mathbf{p}))+\alpha^2\mathbf{L}^T\mathbf{L}\mathbf{p}), \tag{6}$$

where $\mathbf{S}$ is the sensitivity matrix computed using an adjoint field method as in [2, 7, 9]. Equation (6) is usually solved by preconditioned conjugate gradient algorithms.

III. Results

An eight coil system is employed to generate the measurements required for image reconstruction. The coils are arranged in a cylinder with 50 cm of diameter, with equal angular spacing between them, and all of their axis belong to the same plane. All coils have a radius of 3.5 cm, are 4 cm long and have 8 windings equally spaced. In turn, each coil acts as the source and the measurements are acquired by the remaining ones. The number of positions for the training target is 280, which corresponds to ten times the number of linearly independent data points provided by this MIT system.

A. Artificial Phantoms

In figure 1 the electrical conductivity map is reconstructed and the electrical permittivity and magnetic permeability are regarded as known parameters of equal value of the free space properties. Both the developed algorithm and the single-step GN method were used for reconstruction of two spherical perturbations of 1.5 cm of radius and conductivity of 1.5 S/m placed within a 0.5 S/m medium. The values were chosen as such to be in the usual range of biological tissues [12].

Both methods enable the 3D localization of the spherical bodies. However, it is clear that the developed algorithm's reconstruction is more precise when compared to the single-step GN method. The image is less blurry and the ringing artifact, which corresponds to areas of opposite sign surrounding the main reconstructed areas, isn't as evident. The image quality can be more accurately assessed by determining the error $||\mathbf{p}_{true} - \mathbf{p}_{reconstructed}||/||\mathbf{p}_{true}||$, being $\mathbf{p}$ the distributed parameter map. This image error is 35.83% using the single-step GN method and 20.51% using the developed algorithm.

A more challenging reconstruction in which all PEP were estimated was also carried out using the developed algorithm. The same medium is employed but now four spherical bodies are used, with the same diameter and conductivity as previously, but now with relative electric permittivity and magnetic permeability respectively equal to 1600 and 2. The results are displayed in figure 2, where only the $z = 0$ plane is shown. The four objects are clearly identified in all three maps, which is an amazing feature as this is a linear reconstruction. The spherical inclusions closer to the boundary of the medium have a worse reconstruction

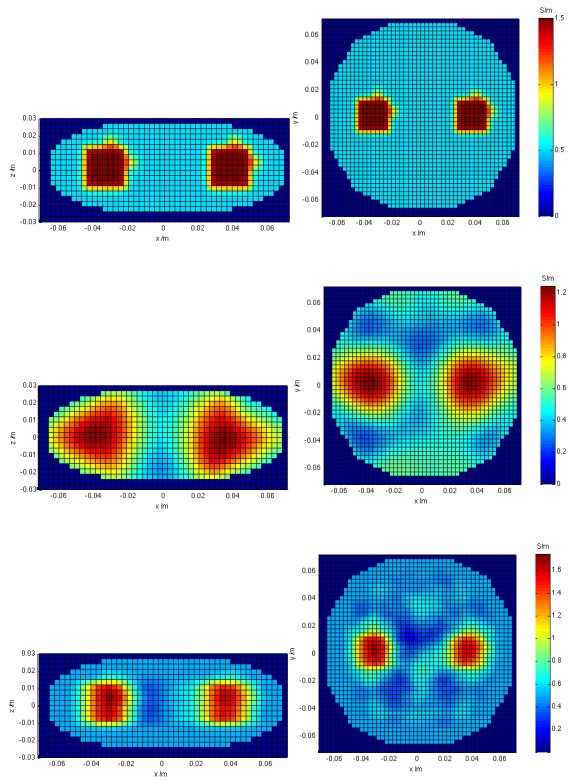

Fig. 1: Reconstructions of the electrical conductivity. Top row: True map; Middle Row: Single-step regularized Gauss-Newton reconstruction; Bottom row: Reconstruction using the developed algorithm. The images are presented in the $y = 0$ (left column) and $z = 0$ (right column) planes.

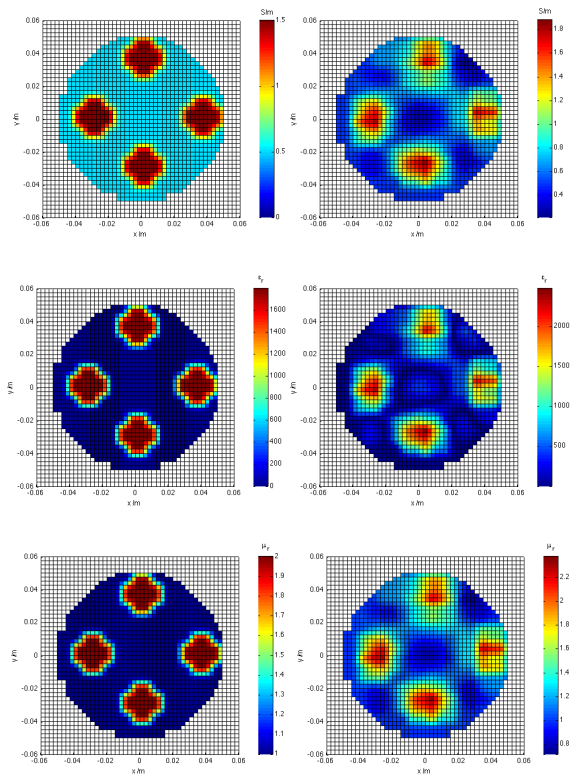

Fig. 2: Reconstruction of the passive electretic properties. Top row: Conductivity maps; middle row: permittivity maps; bottom row: permeability map. The left column represents the original maps and the right column the reconstructed ones.

than the ones closer to the center. This non-uniform resolution could perhaps be solved as in [11], by assigning a wheighting function to each training target to counter the higher sensitivity of the measured data to elements closer to the boundary of the object, which pushes reconstructed noise towards the boundary. The image errors for the three PEP maps are 30.15% (conductivity), 69.97% (permittivity) and 16.64% (permeability). The magnetic permeability map is the one with highest resolution as this is the PEP that affects the magnetic field the most. This is corroborated by [9], where they concluded that the MIT inverse problem is better posed for magnetic permeability reconstructions. The electrical permittivity map is the one with worse resolution and the one with the most image artifacts. This PEP is related to the displacement currents within the object which do not play in MIT a role as significant as the conductive currents dictated by the conductivity distribution. Hence the result is as expected, for the sensitivity of the measurements to conductivity changes is much higher when compared to permittivity changes.

B. Biological Phantoms

A conductivity model of the human head derived from a high resolution magnetic resonance image was developed and used to study the aplicability of the developed algorithm in the clinical enviornment. A k-means algorithm was used to remove any noise outside the region of interest and afterwards a statistical parametric mapping software developed for MatLab was employed to perform the segmentation of the brain tissue into white matter (WM), grey matter (GM) and cerebrospinal fluid (CSF). By combining the resulting binary masks with the denoised data, one was able to obtain as well a mask for the skull voxels, which are modeled as having the same conductivity as bone. Finally, all these masks were combined and assembled after the assignment of the respective tissue's electric conductivity, which is 0.1 S/m, 0.16 S/m, 2 S/m and 0.02 S/m respectively for WM, GM, CSF and bone at 1 MHz of frequency [12]. The magnetic permeability is assumed constant and equal to that of free space, and the electrical properties assigned are assumed homogeneous and isotropic within each tissue. The resulting model is presented in figure 3.

It's composed by cubic voxels of 1 mm side length, which leads to a total number of around one million voxels. A FIT grid of this size is, however, impractible under an MIT framework, as that would imply the resolution of multiple linear systems of size at least three by three times that same number, something that wouldn't be computationally viable. As such, the resolution was decreased five times and each conductive grid element represents the mean value of the complex conductivity contained within it.

The attempted reconstruction scenario consists in a simu-

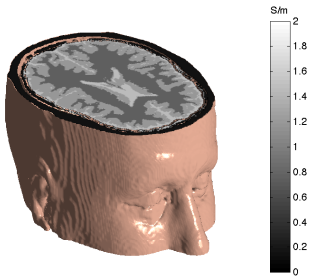

Fig. 3: Conductivity model of a human head. Four different tissues are visible, white matter, grey matter, cerebrospinal fluid and bone.

lated 8 ml subdural heamorrage, located in the right parietal lobe. At the frequency of 1 MHz, the conductivity of blood is 0.8 S/m [12]. For the assembly of the reconstruction matrix it is assumed that the outline of the head is known and the same homogenous conductivity is assigned to all tissues. Afterwards, 280 positions for the spherical perturbation are scanned and the resulting maps and respective measurements are arranged and used in equation (4). Since the projections are taken only on a single plane, the estimation space was restricted vertically to the lower and upper limits respectively of -5 cm and 10 cm, which makes the number of estimated parameters equal to 10232. The original and reconstructed maps are presented in figure 4.

This is a very good result as it is a linear reconstruction of a highly complicated conductivity distribution, severely ill-posed as the number of parameters being estimated is 365 times larger than the number of available measurement data points, and still, the shape and 3D location of the heamorrage is reasonably accurate. The reconstructed conductivity values are fairly close to those in the original map. The main difficulty for reconstructing such distribution map lies in the very high conductivity of the CSF, when compared to the remaining tissues, and the fact that it lies near the boundary.

IV. Conclusions

A linear image reconstructed algorithm was developed and tested. It allowed a reduction of 15% in the image error when compared to the standard single-step GN method. Reconstructions of single or multiple PEP maps are possible through the proposed approach. The algorithm's beahavior under a simulated clinical scenario was considered very promising and it is believed that it can be enhanced even further by increasing the number of independent measurements, as well as the number of target positions.

Acknowledgement

The authors gratefully acknowledge the financial support given by the Portuguese foundation for Science and Technology (FCT) under the grant PTDC/EEA-ELC/105333/2008.

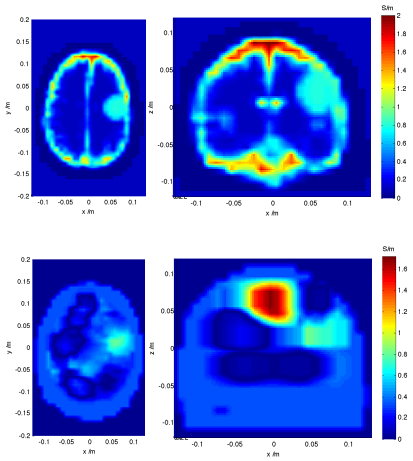

Fig. 4: Reconstruction of a subdural heamorrage located in the right parietal lobe. Top row: the bioimpedance model in which an ellipsoidal object was added to simulate a small hemorrage; Bottom row: reconstructed maps using the new algorithm.

References

[1] H. Huang, T. Takagi, and H. Fukutomi, "Fast signal predictions of noised signals in eddy current testing", *IEEE Trans. Magn.*, vol. 36, no. 4, pt. 1, pp. 17191723, July. 2000.

[2] M. Soleimani, and W. R. B Lionheart, "Absolute Conductivity Reconstruction in Magnetic Induction Tomography Using a Nonlinear Method", *IEEE Transactions on Medical Imaging*, vol. 25, no. 12, pp. 1521-1530, December 2006

[3] S Sapetsky, V Cherepenin, A Korjenevsky, V Kornienko and A Vartanov, "Development of the system for visualization of electric conductivity distribution in human brain and its activity by the magnetic induction tomography (MIT) method", *Journal of Physics*, Conference Series 224, 2010

[4] A. Korjenevsky, V. Cherepenin, and S. Sapetsky, "Magnetic induction tomography: experimental realization", *Physiological Measurements*, vol. 21, pp. 89-94, 2000

[5] H. Griffiths, W. R. Stewart, and W. Gough, "Magnetic induction tomography: a measuring system for biological tissues", *Ann. New York Acad. Sci.*, vol. 873, no. 3, pp.35-45, 1999

[6] R. Casañas, H. Scharfetter et. al, "Measurement of liver iron overload by magnetic induction using a planar gradiometer: Preliminary human results", *Physiol. Meas.*, vol. 25, pp. 315323, 2004.

[7] D. N. Dyck, D. A. Lowther, "A Method of Computing the Sensitivity of Electromagnetic Quantities to Changes in Materials and Sources", *IEEE Trans. Magn.*, vol. 30, no. 5, September 1994

[8] M. Clemens and T. Weiland, "Discrete electromagnetism with the finite integration technique", *Progress In Electromagnetics Research*, PIER 32, pp. 65-87, 2001

[9] M. Soleimani, "Simultaneous Reconstruction of permeability and conductivity in Magnetic Induction Tomography", *J. of Electromagn. Waves and Appl.*, vol. 23, 785798, 2009

[10] Y. Chen, M. Yan, D. Chen, M. Hamsch, H. Liu, H. Jin, M. Vauhkonen, C. H. Igney, J. Kahlert, Y. Wang, "Imaging hemorrhagic stroke with magnetic induction tomography: realistic simulation and evaluation", *Physiological Measurements*, vol. 31, pp. 809-827, 2010

[11] A. Adler, J. Arnold, R. Bayford, A. Borsic, B. Brown, P. Dixon, T. Faes, I. Frerichs, H. Gagnon, Y. Garber, B. Grychtol, G. Hahn, W. Lionheart, A. Malik, R. Patterson, J. Stocks, A. Tizzard, N. Weiler, G. Wolf, GREIT: a unified approach to 2D linear EIT reconstruction of lung images, *Physiol. Meas*, vol. 30, pp. S35S55, 2009

[12] O. G. Martinsen and S. Grimnes, "Bioimpedance and Bioelectricity Basics, Second Edition", *Academic Press*, 2008